Research Article Vol. 30, No. 4 / 14 Feb 2022 / Optics Express 5107
Optics EXPRESS

Efficient transmissive remote phosphor configuration for a laser-driven high-luminance white light source

NICK RONDELEZ,[1,*] ANTÓNIO CORREIA,[1] WOUTER RYCKAERT,[1] HERBERT DE SMET,[2] DIETER CUYPERS,[2] AND YOURI MEURET[1]

[1] KU Leuven, Department of Electrical Engineering (Wavecore), Light & Lighting Laboratory, Gebroeders De Smetstraat 1, 9000 Gent, Belgium
[2] imec and Ghent University, Centre for Microsystems Technology (CMST), Technologiepark Zwijnaarde 126, 9052 Zwijnaarde, Belgium
[*] nick.rondelez@kuleuven.be

Abstract: To realize laser-driven high-luminance white light sources, many reflective configurations have been studied, often resulting in a challenging optical design. In this paper it is demonstrated that the efficacy of a transmissive configuration can be significantly enhanced by using a sapphire half-ball lens as out-coupling optic. This lens not only improves efficiency, but also drastically increases the potential light output due to improved heat dissipation from the single-crystal phosphor converter. Both claims are substantiated with detailed experimental results and realistic opto-thermal simulations, showing a light output of 6550 lm and over 20000 lm, respectively and corresponding luminance of 67 MCd/m^2 and 209 MCd/m^2.

1. Introduction

Solid-state light sources have superior lifetime, efficiency, and switching speed compared to traditional light sources, making them very useful in a large variety of applications such as displays, biomedical devices and general indoor and outdoor lighting [1–4]. The most common method of generating white light for general lighting is using a highly efficient blue LED in combination with one or more down-converting phosphors [5]. The main issue with blue LEDs is that, even though they can have high power conversion efficiencies of over 80 %, this conversion efficiency is strongly dependent on the input current density. For blue LEDs the internal quantum efficiency decreases with increasing current density, an effect which is called power droop.

For lighting applications that require high-luminance light sources, for example car headlights, laser diodes (LDs) are increasingly considered. LDs do not suffer from power droop. On the contrary, their power-conversion efficiency increases with increasing current density [6]. In addition, laser diodes have a small emitting surface and limited beam divergence. As a result, much optical power can be emitted within a very limited étendue. Such low-étendue light sources make it more straightforward to realize accurate tailoring of the emitted light with compact optical components [7], and thus develop compact illumination systems as for examples in car headlamps [8] and street lighting.

Similar as with LEDs, a down-converting/yellow-emitting phosphor is typically used to generate white light with blue laser diodes. For a laser-driven white light source this is typically a remote phosphor, at a certain distance from the LDs. In order to adopt such a down-converting phosphor in a high-luminance LD-based white light source, an important consideration needs to be made. When a fluorescent material is used, the imperfect quantum yield (QY) and Stokes-shift always result in thermal energy losses. This manifests itself as an increase of the fluorescent material temperature. In the case of LDs however, the incident optical flux density can be very

#449016 https://doi.org/10.1364/OE.449016
Journal © 2022 Received 24 Nov 2021; revised 21 Jan 2022; accepted 24 Jan 2022; published 2 Feb 2022

Optics EXPRESS

high. As the thermal conductivity of traditional color converters is rather low, this can result in thermal damage [9,10]. Novel color converter materials with improved thermal conductivity and higher damage threshold, such as phosphor ceramics [11–14] and single crystal phosphors [15–19], are therefore intensively investigated at this moment. However, even with these novel color converter materials there is still a significant increase of temperature when illuminated by high-power LDs. This increase in temperature pushes down the QY of the phosphor, a phenomenon which is called thermal quenching. The reduced QY furthermore increases thermal losses, which in turn, further increases temperature. This feedback loop can cause a thermal runaway inside the color converter material, with a severely reduced efficiency or even thermal damage as result. When using (remote) phosphor materials, good thermal dissipation is thus extremely important to ensure thermal stability and high efficiency of the emitted light.

In the literature, many examples can be found of white light sources that are based on the illumination of a remote phosphor layer by one or more, typically blue, high power laser diodes. Many of these configurations use a reflective approach, in which the phosphor material is placed onto a reflective heatsink. The main advantage of a reflective configuration [20–23] is that the phosphor is in thermal contact with the heatsink, effectively cooling the fluorescent material and thereby preventing thermal runaway. A disadvantage of reflective configurations however, is that the LDs and collimation optics are on the same side of the color converter. This significantly complicates the optical design [20,23]. Transmissive configurations [10,24–27] solve this problem, because the illumination beam and collimation optics for the color converted light are on opposite sides of the color converter. In transmission however, thermal management is much more difficult. To limit the temperature of the color converter, different approaches have been tested from developing robust light converters [24] to using transparent highly thermally conductive materials like Al_2O_3 [10,26]. Another important problem of transmissive configurations is that the converted light can exit the color converter at two sides. This imposes a serious limitation on the overall system efficiency. Zheng et al. [10] and Tang et al. [27] both incorporated a short-pass filter on the entrance side of the color converter and long-pass filter on the exit side to ensure maximum conversion of the incident blue light and to limit the amount of back-reflected light. Applying these multi-layer coatings however, does not resolve the thermal issues in any way.

In this paper we present a blue LD-based high-luminance, étendue-limited white light source with a remote phosphor layer. A novel transmissive configuration is introduced that provides a solution to both the optical and thermal challenges of the transmissive approach. By bringing a sapphire half-ball lens in optical contact with a single crystal YAG:Ce phosphor plate, most of the down-converted light that would otherwise be trapped in the high-refractive index layer, is now coupled-out in the forward direction. This preferential out-coupling in the transmissive direction boosts the optical efficiency of the system significantly. The sapphire half-ball lens is also very effective in conducting the generated heat away from the thin phosphor plate. The optical and thermal advantages of the presented transmissive LD-based configuration for generating high-luminance white light are analyzed in detail with both optical and opto-thermal simulations, and are validated with experimental measurements.

2. Investigated optical / thermal configuration

For obtaining an étendue-limited, high-luminance white light source, the system from Fig. 1 is investigated. A four-by-four blue LD array emits sixteen beams of blue, collimated light. A focusing lens aims the individual laser beams into the entrance aperture of a reflective compound parabolic concentrator (CPC). A CPC is a very effective concentrator that converts the incident light beam into a light beam with smaller spatial extent and larger angular extent, but with the same étendue [28]. At the exit of this CPC, a thin, single crystal phosphor plate is placed that efficiently converts part of the incident blue light into yellow light. Finally, a sapphire half-ball lens is brought in optical / thermal contact with this phosphor plate.

Optics EXPRESS

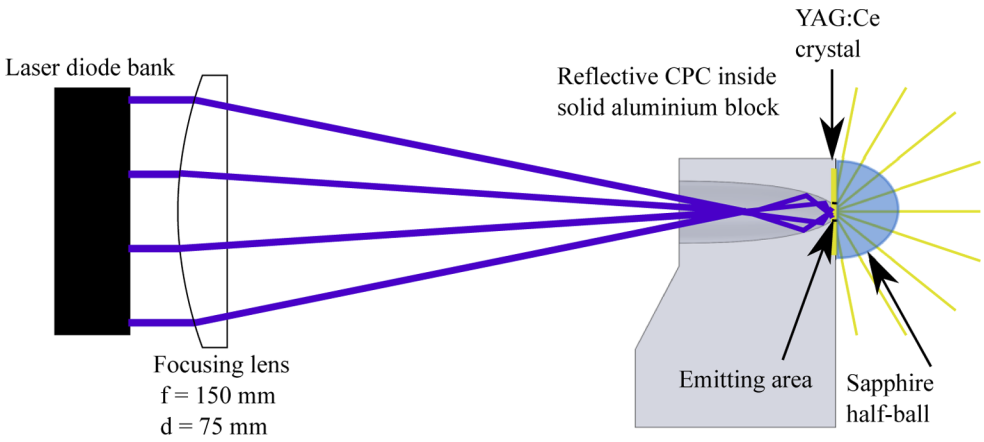

Fig. 1. Schematic of the investigated optical/thermal configuration for generating high-luminance, low-étendue white light.

The blue laser diode array consists of two LD banks of each 8 individual LDs. The complete array can emit up to 76 W of optical power at a peak wavelength of 455 nm. The focal length and diameter of the anti-reflective (AR)-coated focusing lens are 150 mm and 75 mm respectively, resulting in a maximal half beam angle of 15° for the incident laser light at the CPC entrance. The CPC was designed for an input half angle of 15° and output half angle of 90°. The entrance aperture has a diameter of 11.59 mm, the exit aperture of 3 mm. The reflective CPC was machined in a solid aluminium block via CNC-milling. This milling process gave rise to a sub-optimal surface reflectivity and surface roughness. As a result, a transmission efficiency of only 57.1 % was reached. At maximal incident power, this resulted in a power density of 5.9 W/mm^2 at the exit of the CPC. A more advanced fabrication and coating method for the CPC inside the aluminium block could well increase the transmission efficiency to around 95 %, e.g. by manufacturing the component as two separate parts, that are merged after electroplating.

The CPC was manufactured inside a solid block of aluminium such that the large volume of aluminium could be used as a heat sink for the generated thermal energy inside the phosphor crystal. A square cutout was made in the aluminium block just after the CPC exit, in order to position a 0.2 % wt Cerium(III)-doped Yttrium Aluminium Garnet (YAG:Ce) single crystal phosphor (SCP) with dimensions 10 mm × 10 mm × 0.5 mm. The SCP (provided by PI-KEM) was brought in thermal contact with the aluminium block by using thermal paste away from the CPC exit. Finally, a sapphire half-ball lens with a diameter of 20 mm was brought in optical and thermal contact with the SCP, in order to increase the amount of out-coupled light in the forward direction and improve heat dissipation away from the SCP. The SCP with sapphire half-ball lens on top is shown in Fig. 2 (left).

The ideal approach to bring the SCP and sapphire half-ball lens in perfect optical and thermal contact would be via optical contact bonding. Optical contact bonding however requires that the surfaces are extremely flat, smooth and clean [29]. A maximal flatness of $\lambda/10$ is needed along with a root mean square surface roughness of around or below 1 nm [30]. The surface flatness and roughness of the SCP and sapphire half-ball lens were therefore characterized with a mechanical stylus profilometer (Tencor Alphastep 200) and optical profilometer (Veeco Wyko NT3300), respectively The measured RMS surface roughness of the crystal was found to be 0.3573 nm and the surface warpage is displayed in Fig. 2 (Right). We thus found that the surfaces of both components were not sufficiently flat and had a significant degree of surface warpage. Due to this warpage, the center of both components do not touch, making optical contact bonding

Optics EXPRESS

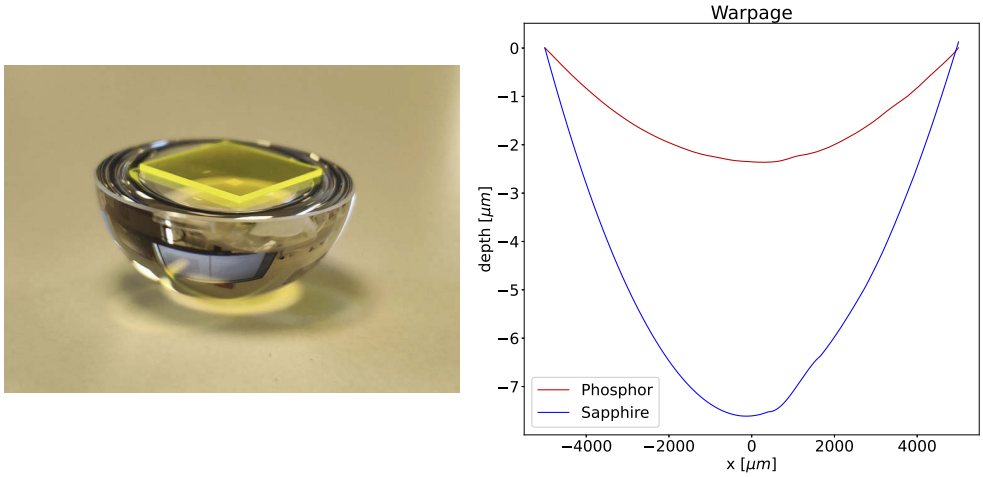

Fig. 2. (Left) Image of YAG:Ce SCP and sapphire half-ball lens. (Right) Measured warpage for polished surfaces of half-ball lens and SCP, clearly illustrating the gap between both components. A RIL fills up this gap and ensures optical contact.

impossible. A more accurate fabrication method for both the SCP and sapphire half-ball lens would thus be needed to realize optical contact bonding.

To bypass the limitations of the components, a refractive index liquid (RIL) [31] is used between the SCP and sapphire half-ball lens. From an optical point of view, this approach is very similar to optical contact bonding, provided that the refractive index of the liquid (1.7939 @ 530 nm) is between that of YAG:Ce (1.8383 @ 530 nm) and sapphire (1.7718 @ 532 nm). The main drawback of the RIL is that it can only be used for relatively low temperatures up to 110 °C. This approach thus imposes certain thermal limitations that are further discussed in section 4.

The converted light inside the SCP is emitted in an isotropic manner. The half-ball lens in optical contact with the SCP avoids total internal reflection (TIR) of the converted light at the right/exit side of the SCP, while TIR is still present on the left/entry side of the SCP. This lens thus maximizes out-coupling of yellow-converted light in the forward direction.

The used phosphor plate is very thin (only 0.5 mm), so the spatial extent of the (converted) light that exits the SCP in the forward direction is very similar to that of the exit aperture of the CPC. To accurately model the emitting area, the further discussed LightTools model was used. We found that for the YAG:Ce crystal alone, 90% of the luminous flux is emitted from a circle with radius equal to 1.10 mm, while for the case with sapphire half-ball lens this radius is equal to 1.78 mm. The étendue of the emitted light in the forward direction can, to a good approximation, be calculated using

$$\epsilon = \pi \cdot n^2 \cdot r^2 \cdot \pi \cdot \sin^2\theta \tag{1}$$

For the YAG:Ce crystal alone, the refractive index of air ($n = 1$) should be chosen, while for the case with sapphire half-ball lens, n should be equal to 1.7718. In both cases $\theta = 90°$. This gives an étendue of 12 mm^2 for the case without sapphire half-ball lens and an étendue of 98 mm^2 for the case with half-ball lens. These étendue values are later on used to calculate the average luminance of the emitted light in the forward direction.

Optics EXPRESS

3. Simulation models

3.1. Optical simulations

The complete optical configuration was implemented and analyzed in the LightTools ray-tracing software [32]. The laser beams, focusing lens and reflective CPC were modelled in a straightforward manner: the laser beams as perfect collimated ray-bundels, the focusing lens as a smooth optical component with perfect transmission and the CPC as a specular reflector with a specific reflectance that is discussed further.

An essential element of the analysis of the optical performance is the single crystal phosphor plate. Fluorescent materials have wavelength dependent properties, which need to be well defined to simulate their behaviour accurately. The spectral absorption coefficient $\mu_a(\lambda)$ should be known along with the corresponding emission spectrum and quantum yield (QY). The QY of the phosphor is the ratio of converted to absorbed photons. Both QY and emission spectrum at room temperature were experimentally measured using an integrating sphere setup as described in [33]. This resulted in a QY of 0.96 and an emission spectrum with a peak wavelength around 540 nm as shown in Fig. 3 (left).

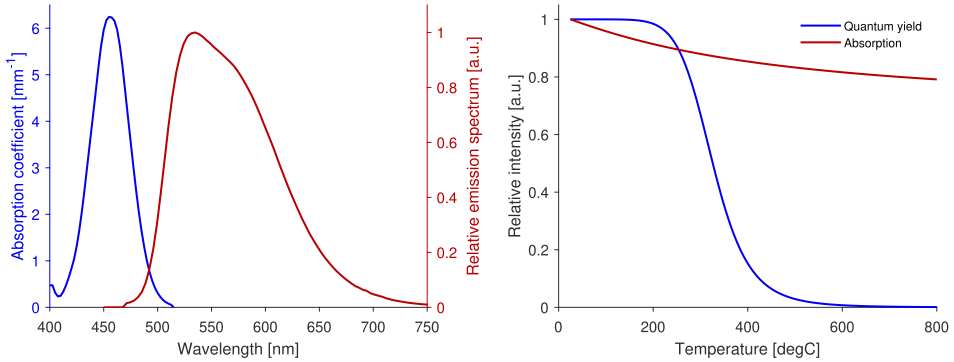

Fig. 3. Used values for the optical properties of the single crystal YAG:Ce phosphor plate. (Left) The absorption coefficient and relative emission spectrum at room temperature. (Right) The variation of the relative quantum yield and peak absorption coefficient with temperature [34].

Determination of the spectral absorption coefficient was achieved by placing the phosphor plate in the path of a supercontinuum laser (Fianium, NKT Photonics). The sample was illuminated with different narrow wavelength bands, selected with a monochromator (SuperK VARIA, NKT Photonics) [35]. In the path of the supercontinuum laser and SCP, a spectrometer (Instaspec IV, Oriel Instruments) was placed to capture the undeviated transmitted light from the supercontinuum laser. The measured spectral power density is then compared to the case where the SCP was not in the supercontinuum laser path. The data obtained in these measurements was processed to get approximate values for the spectral extinction coefficient $\mu_t = \mu_s + \mu_a$, with μ_s and μ_a the scatter and absorption coefficient, respectively. Since a non-scattering single crystal is used, the scatter coefficient $\mu_s = 0$ so that $\mu_t = \mu_a$. Applying the Beer-Lambert law and taking Fresnel reflections at the interfaces into account gives an expanded series to solve the absorption coefficient, given in Eq. (2).

$$\Phi_o(\lambda) = \Phi_i(\lambda) \cdot \frac{(1 - R(\lambda))^2 \cdot e^{-\mu_a t}}{1 - R(\lambda)^2 \cdot e^{-2\mu_a t}} \tag{2}$$

Φ_o and Φ_i are the measured spectral power density after the crystal and without the crystal, respectively. $R(\lambda)$ is the spectral reflection determined by the wavelength-dependent refractive

Optics EXPRESS

index and t is the thickness of the SCP. The extracted spectral absorption coefficient can also be seen in Fig. 3 (left).

3.2. Opto-thermal simulations

The focusing of multiple LDs in a circular area with a diameter of 3 mm causes large power densities inside the SCP. Fluorescent conversion inside the crystal generates heat which will increase the temperature of the crystal. A major challenge in accurately simulating luminescent materials is that the optical properties of these materials (e.g. QY and absorption coefficient) are strongly temperature-dependent. This results in a complex interplay between the QY, absorption coefficient and temperature. To take this interplay into account, a holistic time-resolved opto-thermal simulation framework (hOTS) [36] was developed to model both the optical and thermal performance of such systems. The framework introduces a feedback loop, where the optical performance is evaluated in LightTools and fluorescent conversion losses within luminescent materials are monitored. This information is then used in COMSOL Multiphysics [37] to simulate the temperature distribution of the considered system. For every time-incrementation, the temperature-dependent optical properties are adjusted within the optical simulation software, in order to use the QY and absorption corresponding to the current temperature. By taking the temperature increase as a function of time into account, the moment at which the optical performance starts to decrease can be predicted and the limits of the system can be accurately determined. The variation of the QY and absorption coefficient as a function of temperature for the considered SCP, are shown in Fig. 3 (right) and these values were validated in previous work [36]. When fluorescent materials are excited by a very high photon density, optical luminescence quenching can also occur. For YAG:Ce it is reported that this only happens at power densities from 10-50 W/mm^2 [38]. So while this effect can be simulated in hOTS, it has not been observed in our experiments and was therefore not included in the simulations.

Two opto-thermal configurations are analyzed and compared. The first configuration consists of the aluminium holder with a reflectivity of 95 % and SCP, illuminated by the LD array. The exposed surfaces dissipate thermal energy by radiation and convection. The heating process of the SCP occurs in two steps. When the laser beam is turned on, temperature inside the crystal increases rapidly, reaching a first steady-state temperature in less than 1 s to a couple of seconds, depending on the incident radiant flux. Since the SCP is in good thermal contact with the aluminium holder, the temperature of this holder slowly increases due to the spreading of the heat generated in the SCP. Depending on the illumination power and the cooling method for the aluminium block, this second heating process can take minutes to hours to reach a final steady state. Assuming proper cooling of the aluminium block, the simulation model assumes that the aluminium temperature is kept constant at room temperature. This assumption has limited impact on the thermal dynamics of the SCP which occur at much higher temperatures than the aluminium temperature.

The second configuration consists of the aluminium holder, SCP and sapphire half-ball lens in optical/thermal contact with the SCP. In this case, the high thermal conductivity of sapphire improves the dissipation of thermal energy away from the SCP, as will be discussed further. Table 1 shows the thermal properties of all considered components.

Using the hOTS framework, the opto-thermal performance is evaluated for a variety of radiant fluxes incident on the SCP. First, the study is conducted in case QY and absorption are assumed temperature-independent, for reasons of simplicity. Next, a realistic transient study is done where both QY and absorption are adjusted in a feedback loop.

Optics EXPRESS

Table 1. Thermal properties of the components used in the thermal simulations using COMSOL Multiphysics 5.2a

Property	YAG:Ce	Al_20_3
Thermal emissivity	0.83	0.48 [39]
Thermal conductivity	11.2 W/(m · K) [40]	25.2 W/(m · K) [41]
Density	4560 kg m^{-3} [40]	3980 kg m^{-3} [41]

4. Results and discussion

4.1. Optical performance

The optical performance evaluation is separated in two parts. First, optical simulations are performed taking the measured optical properties of YAG:Ce into account. Two different situations are considered: a case where the reflectivity of the CPC is chosen to match the measured transmission efficiency of only 57 %, and a case where this reflectivity is chosen equal to 95 %. The latter enables us to evaluate the potential optical efficiency that the system has to offer. In a second part, measurements of the optical system are conducted at low power, in a regime where no thermally induced changes of the optical properties arise. The measured spectral power density with and without sapphire half-ball lens are evaluated and compared with the optical simulations.

4.1.1. Simulation results

Simulations are conducted with LightTools as described in section 3.. In order to approximate the measured configuration, the CPC reflectivity was assumed to be equal to 55 % in order to have a simulated transmission efficiency of 57 %. For this configuration, four different spectral power densities (SPD) are simulated. First, the SPD after the focusing lens is simulated. Second, the SPD is evaluated at the output of the CPC. Then the SPD is simulated at the output of the phosphor crystal without sapphire half-ball lens. And finally the SPD is evaluated at the output of the system when a sapphire half-ball lens is brought in optical contact with the phosphor crystal. In order to calculate the luminous efficacy K and efficiency η, the total luminous and radiant flux corresponding with these four SPD's, are respectively divided by the radiant flux emitted by the blue LDs. The resulting values are shown in Table 2, together with the corresponding CCT. Luminous efficacy and CCT however, are only provided for the cases where the phosphor crystal is included in the simulation.

Table 2. Simulation results when CPC reflectivity equals 55 %. Luminous efficacy (K), optical efficiency (η) and CCT are simulated using 10 M rays. Without color conversion, the CCT and luminous efficacy are not relevant (-).

	K	η	CCT
After focusing lens	-	98.7 %	-
After CPC	-	55.3 %	-
After phosphor crystal	41.0 lm/W	11.0 %	5860 K
After sapphire half-ball lens	119 lm/W	27.2 %	4836 K
Improvement with half-ball lens	191 %	148 %	-

Using the sapphire half-ball lens in optical contact with the phosphor crystal clearly increases the amount of out-coupled light. An optical efficiency of 11.0 % and 27.2 % are obtained respectively, without and with the sapphire lens. This is a 148 % improvement of the emitted radiant flux. The luminous efficacy K of the light source improves from 41.0 lm/W to 119 lm/W.

Optics EXPRESS

The change in CCT from 5860 K to 4836 K confirms that especially additional yellow light is coupled out.

To evaluate the potential efficiency of the proposed configuration, a CPC with a higher reflectivity of 95 % is considered. Table 3 shows the simulated luminous efficacy, optical efficiency and CCT as before. It is again clear that using the sapphire half-ball lens increases the amount of out-coupled light. The luminous efficacy is increased from 68.5 lm/W to 201 lm/W, an improvement of 192 %. The optical efficiency improves by 148 %. It is clear that the CPC reflectivity has an influence on the overall efficiency and luminous efficacy, as is to be expected. However, it does not affect the efficiency and luminous efficacy improvement with half-ball lens in any way. The average simulated CCT with a sapphire lens is 4834 K.

Table 3. Simulation results when CPC reflectivity equals 95 %. Luminous efficacy (K), optical efficiency (η) and CCT are simulated using 10 M rays. Without color conversion, the CCT and luminous efficacy are not relevant (-).

	K	η	CCT
After focusing lens	-	98.7 %	-
After CPC	-	93.9 %	-
After phosphor crystal	68.5 lm/W	18.4 %	5867 K
After sapphire half-ball lens	201 lm/W	45.7 %	4834 K
Improvement with half-ball lens	192 %	148 %	-

4.1.2. Experimental validation

The high-power LD banks are mounted on a heatsink and cooled with active CPU cooling as shown in Fig. 4. The measurements are conducted at low-power (a current of 0.5 A, corresponding with an emitted radiant flux of 4.56 W) with a calibrated integrating sphere setup. Under these driving conditions, the emitted radiant flux from the SCP is stable, while the SCP temperature remains below 50 °C.

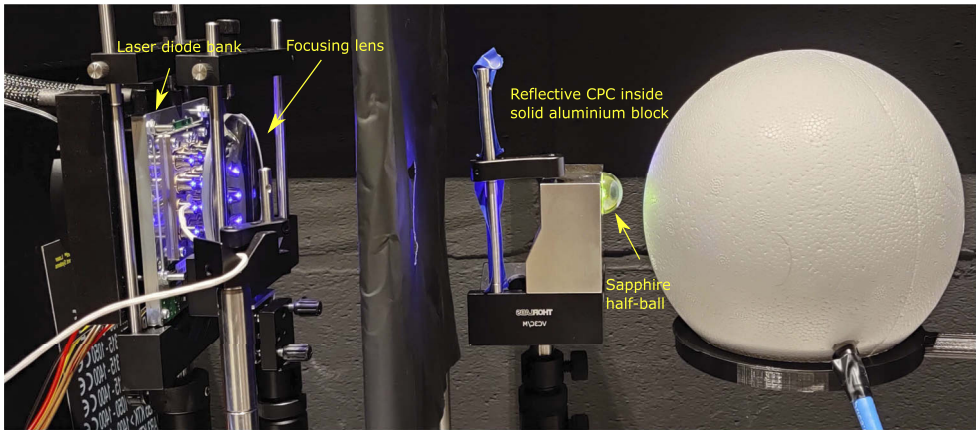

Fig. 4. Measurement setup with calibrated integrating sphere

The measured efficiencies are summarized in Table 4 and these confirm that utilizing an out-coupling optic significantly increases the amount of out-coupled optical flux. The measured optical efficiency increases by 146 %, from 9.9 % to 24.5 %. The luminous efficacy is improved

Optics EXPRESS

by 192 %. The measured spectral power density in Fig. 5 shows that the increase in optical flux can be fully attributed to the reduction of yellow-converted light trapping.

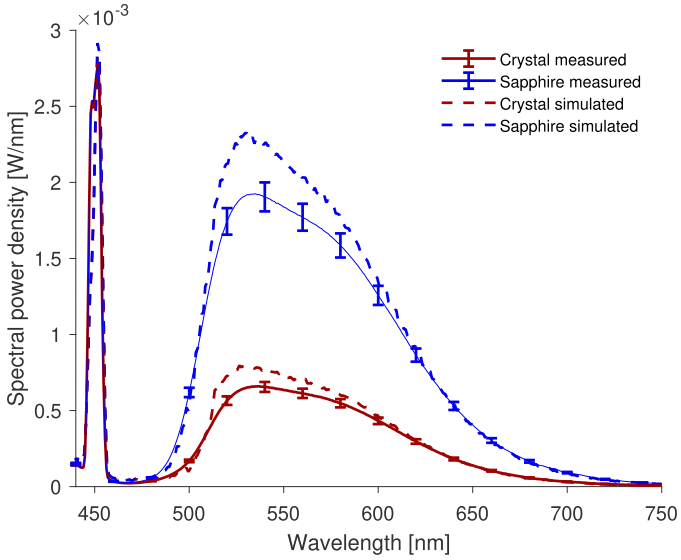

Fig. 5. Measured and simulated spectral power density from the SCP with and without sapphire half-ball lens. The sapphire lens clearly improves the out-coupling of yellow-converted light. The error on measurement data is +/- 5 %. Simulations of the optical configuration are performed in LightTools 8.7.0.

Table 4. Measured optical efficiency comparison for added components to the CPC holder. η_{cpc} is the CPC efficiency compared to the reference beam. The other efficiencies are compared to the output power after the CPC and finally the out-coupling improvement is represented.

	K	η	CCT
After focusing lens	-	100 %	-
After CPC	-	57.1 %	-
After phosphor crystal	36 lm/W	9.9 %	5880 K
After sapphire half-ball lens	105 lm/W	24.5 %	4729 K
Improvement with half-ball lens	192 %	146 %	-

The LightTools model proves to be sufficiently accurate in order to predict the optical behaviour of the configuration and maximum power output which can be obtained. However, some differences are observed. We suspect that this difference is due to the measurement method making it impossible to measure all emitted light, especially for extreme angles of the forward hemisphere. This results in a slightly higher absolute efficiency compared to measurements.

4.2. Opto-thermal performance

While the previous section described the simulated and measured efficiency of the considered light source, the total luminous flux that could be produced with such a system is not elaborated. For this, the opto-thermal performance of the system should be evaluated. This opto-thermal performance evaluation is separated in two parts. First, opto-thermal simulations are performed to analyse the impact of temperature on the efficiency of the system, with and without sapphire

Optics EXPRESS

half-ball lens. In doing so, the maximal potential light output and corresponding luminance values of the investigated system can be predicted. In a second part, measurements of the laser-based white light source are conducted at high laser power, in order to assess the practical light output values that can be reached with the current system.

4.2.1. Simulation results

The opto-thermal simulations are performed with the hOTS framework as described in section 3.. The case with CPC reflectivity equal to 95 % is considered. The evolution of the maximum temperature within the crystal is evaluated and displayed in Fig. 6 for different laser output powers. On the left, the time-dependent temperature increase is shown when the emitted LD output power is equal to 24 W, 32 W (+33 %) and 40 W (+66 %). Raising the laser power by 33 % and 66 %, causes the steady-state temperature to increase from 256 °C to 435 °C and 761 °C, respectively. Fig. 6 (right) shows that when the incident amount of radiant flux on the phosphor plate without sapphire half-ball lens is below 24 W, the simulated steady-state temperature with temperature-independent optical properties, overlaps with the simulated steady-state temperature with temperature-dependent optical properties. Beyond an emitted radiant flux of 24 W, this is no longer the case, and simulations with temperature-dependent optical properties result in much higher steady-state temperatures than when these temperature dependencies are not taken into account. The 24 W corresponds with a steady-state temperature of around 250 °C; exactly the point at which the QY starts to drop significantly (see Fig. 3, right). Illuminating the phosphor crystal with a radiant flux larger than 24 W will push temperature higher and QY even lower, resulting in very strong temperature increments.

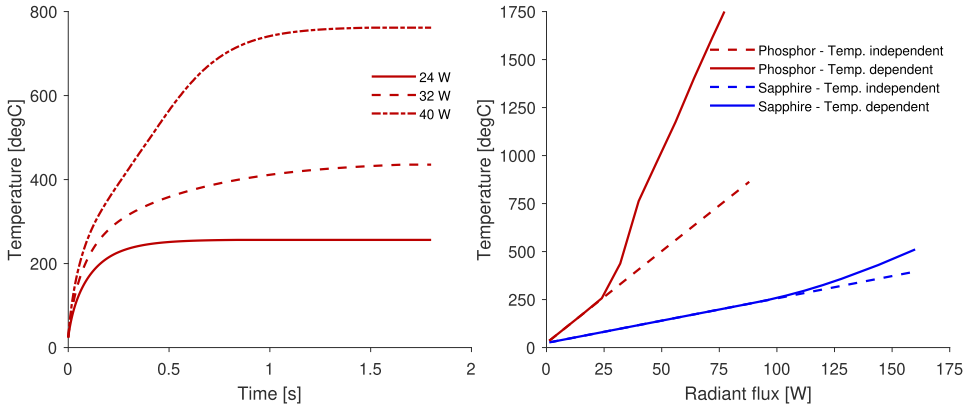

Fig. 6. (left) Temperature as a function of time when temperature-dependent optical properties are considered, for different laser illumination powers. (right) Evolution of the steady-state temperature as a function of the laser illumination power. In the temperature-independent case, QY and absorption are assumed to be constant. In the temperature dependant case, QY and absorption are adjusted and matched to the current local temperature using a feedback loop.

Thermal quenching can also be identified by looking at the evolution of the luminous efficacy as a function of time in Fig. 7, left. Without thermal quenching (16 W), the luminous efficacy remains constant. However, when the incident radiant flux is increased to 24 W, luminous efficacy slightly decreases over time, indicating that thermal quenching is starting to occur. Higher powers further decrease the luminous efficacy. For example, using the LDs at full power (76 W) lowers luminous efficacy from 68.5 lm/W to 27.8 lm/W for the SCP without sapphire lens.

With the sapphire lens in thermal contact with the SCP, the increase in temperature is significantly lower as compared to the SCP alone. The sapphire lens, due to its high thermal

Optics EXPRESS

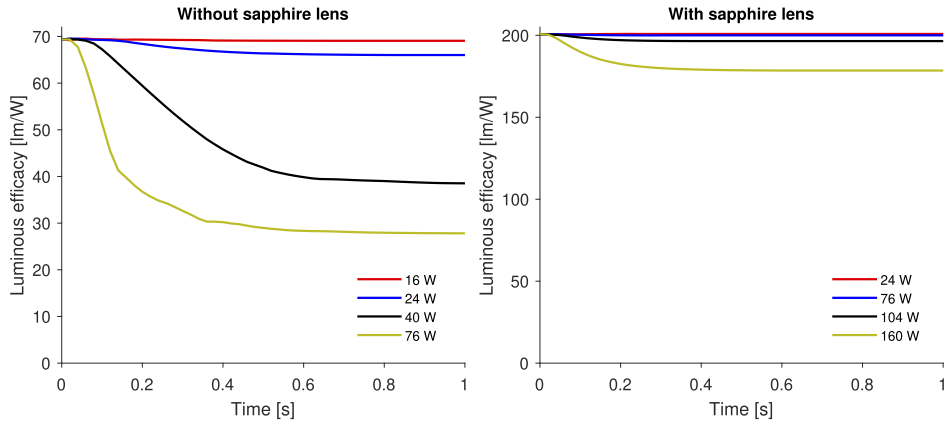

Fig. 7. Evolution of the luminous efficacy as a function of time for four different laser illumination power levels, for (left) the SCP without sapphire lens and (right) the SCP with sapphire lens.

conductance, can extract more heat from the crystal than when it is exposed to air. This extracted heat is then conducted to the aluminium heat sink with which the sapphire half-ball lens is also in thermal contact. This results in an LD radiant flux of 104 W before thermal quenching starts to occur. Even with this amount of radiant flux, the decrease in luminous efficacy is limited. Using 160 W of radiant flux causes a decrease in luminous efficacy from 201 lm/W to 179 lm/W. In addition, Fig. 7 illustrates once more the large influence of the sapphire lens on the amount of out-coupled luminous flux. Where the maximum luminous efficacy for the SCP without sapphire lens is 68.5 lm/W, it is 201 lm/W for the system with sapphire lens.

When establishing the thermal limitations within which the system can operate, several cases are relevant. In order to prevent thermal quenching, it is important that the maximal temperature inside the SCP remains below 250 °C. In the case of the SCP without sapphire lens, this imposes a clear limitation of 24 W for the incident radiant flux. Beyond this value, there is a severe reduction of the luminous efficacy. For the case with sapphire lens, the 250 °C-limit results in a maximal radiant flux of 104 W. In this case, the impact of higher flux levels on the resulting luminous efficacy is more modest. When considering the practical light source that was realized in our lab, another thermal limitation has to be considered. The maximum temperature of the RIL that is used in between the CSP and sapphire lens is 110 °C in order to prevent it from burning. This results in a maximal radiant flux of 40 W. The corresponding luminous flux and average luminance, for each of these maximal radiant flux values can be found in Table 5. The average luminance is calculated using $L_v = \Phi_v/\epsilon$ with Φ_v the luminous flux and ϵ the system étendue, previously calculated. Independent of the configuration and used power, very high luminances from $\approx 16\,\mathrm{MCd/m^2}$ to $\approx 209\,\mathrm{MCd/m^2}$ are attainable.

4.2.2. Experimental validation

The opto-thermal simulations showed that for the case without sapphire lens, it should be possible to increase the incident flux onto the SCP to 24 W before thermal quenching occurs. However, due to the high radiant flux incident on a small area of the SCP, temperature locally rises significantly causing a large temperature gradient within the crystal. This results in a large surface tension, which shatters the crystal before reaching this 24 W of incident radiant flux (i.e. at an incident power level of around 16 W). It was observed in practice that the addition of the sapphire lens also improved the mechanical stability of the SCP at higher temperatures. This prevents the SCP to be shattered at incident radiant flux levels of at least 30 W. When driving the laser diodes with

Optics EXPRESS

Table 5. Summary of the output luminous flux Φ_v and luminance L_v, corresponding to the maximum laser illumination power Φ_e to stay below the specified temperatures.

Max. Φ_e	110 °C (flash point)	250 °C (T quenching)
SCP	NA	24 W
SCP +Al_2O_3	40 W	104 W
Max. Φ_v		
SCP	NA	1585 lm
SCP +Al_2O_3	1533 lm	20435 lm
Max. L_v		
SCP	NA	132 MCd/m^2
SCP +Al_2O_3	16 MCd/m^2	209 MCd/m^2

a current of 2 A, the emitted luminous flux from the sapphire lens exit surface was measured to be 6550 lm with an average CCT of 4729 K. The luminance in this case was 67 MCd/m^2. Currents larger than 2 A caused the RIL to turn brownish-red due to the high irradiance (over 5 W/mm^2) on one of the main components of the RIL (diiodomethane), liberating iodine. This happens before reaching the flash point of the oil and is the current limiting factor. In order to go to higher output powers, optical contact bonding of the SCP with the sapphire half-ball lens would be needed.

5. Conclusion

A novel high luminance light source using laser diodes in combination with a remote single crystal phosphor (SCP) operated in transmission, is designed and developed. The optical and opto-thermal performance of the proposed system is evaluated by simulations and experiments. In doing so, it was demonstrated that the addition of a sapphire half-ball lens in optical and thermal contact with the SCP, improves both the optical and thermal performance of the system. The lens enables extracting light which would otherwise be trapped inside the SCP by total internal reflection. Optical simulations and measurements both show that the emitted amount of radiant flux can be increased by more than 150 %, allowing a theoretical luminous efficacy of over 201 lm/W. The opto-thermal simulations also show that the sapphire lens is beneficial for the extraction of the generated heat inside the SCP. The sapphire lens ensures that the SCP temperature is lower, making it less prone to thermal quenching. The radiant flux at which thermal quenching starts to occur is four times larger than without sapphire lens, allowing a luminous output flux of over 20000 lm (a close to 1200 % increase compared to the SCP alone). The output power of the practical system that was developed in the lab, is currently limited by the need to use a RIL between CSP and sapphire lens. Still, we managed to emit 6550 lm from a circular region with a diameter of 3 mm, with the current setup. To increase this luminous flux further, optical contact bonding of the SCP with the sapphire lens would be required.

Funding. KU Leuven.

Acknowledgements. The authors want to specially thank Dr. Peter Janssens for his insightful comments.

Disclosures. The authors declare no conflicts of interest.

Data availability. Data underlying the results presented in this paper are not publicly available at this time but may be obtained from the authors upon reasonable request.

References

1. H. S. Wasisto, J. D. Prades, J. Gülink, and A. Waag, "Beyond solid-state lighting: Miniaturization, hybrid integration, and applications of gan nano-and micro-leds," Appl. Phys. Rev. **6**(4), 041315 (2019).

Optics EXPRESS

2. R. Pode, "Organic light emitting diode devices: An energy efficient solid state lighting for applications," Renew. Sustain. Energy Rev. **133**, 110043 (2020).
3. R. Haitz and J. Y. Tsao, "Solid-state lighting:'the case'10 years after and future prospects," phys. stat. sol. (a) **208**(1), 17–29 (2011).
4. N. G. Yeh, C.-H. Wu, and T. C. Cheng, "Light-emitting diodes-their potential in biomedical applications," Renew. Sustain. Energy Rev. **14**(8), 2161–2166 (2010).
5. N. C. George, K. A. Denault, and R. Seshadri, "Phosphors for solid-state white lighting," Annu. Rev. Mater. Res. **43**, 481–501 (2013).
6. J. J. Wierer Jr, J. Y. Tsao, and D. S. Sizov, "Comparison between blue lasers and light-emitting diodes for future solid-state lighting," Laser Photonics Rev. **7**(6), 963–993 (2013).
7. K. Desnijder, P. Hanselaer, and Y. Meuret, "Flexible design method for freeform lenses with an arbitrary lens contour," Opt. Lett. **42**(24), 5238–5241 (2017).
8. L. Wang, J. Ma, P. Su, J. Huang, and S. Gu, "A new integrated led automotive headlight with laser supplement light," Proc. SPIE **11548**, 1154821 (2020).
9. Y. Ma, W. Lan, B. Xie, R. Hu, and X. Luo, "An optical-thermal model for laser-excited remote phosphor with thermal quenching," Int. J. Heat Mass Transfer **116**, 694–702 (2018).
10. P. Zheng, S. Li, L. Wang, T.-L. Zhou, S. You, T. Takeda, N. Hirosaki, and R.-J. Xie, "Unique color converter architecture enabling phosphor-in-glass (pig) films suitable for high-power and high-luminance laser-driven white lighting," ACS Appl. Mater. Interfaces **10**(17), 14930–14940 (2018).
11. M. He, J. Jia, J. Zhao, X. Qiao, J. Du, and X. Fan, "Glass-ceramic phosphors for solid state lighting: a review," Ceramics Int. **47**(3), 2963–2980 (2021).
12. S. Li, D. Tang, Z. Tian, X. Liu, T. Takeda, N. Hirosaki, F. Xu, Z. Huang, and R.-J. Xie, "New insights into the microstructure of translucent caalsin 3: Eu 2+ phosphor ceramics for solid-state laser lighting," J. Mater. Chem. C **5**(5), 1042–1051 (2017).
13. S. Li, Q. Zhu, D. Tang, X. Liu, G. Ouyang, L. Cao, N. Hirosaki, T. Nishimura, Z. Huang, and R.-J. Xie, "Al 2 o 3–yag: Ce composite phosphor ceramic: a thermally robust and efficient color converter for solid state laser lighting," J. Mater. Chem. C **4**(37), 8648–8654 (2016).
14. Y. H. Song, E. K. Ji, B. W. Jeong, M. K. Jung, E. Y. Kim, C. W. Lee, and D. H. Yoon, "Design of laser-driven high-efficiency al2o3/yag: Ce3+ ceramic converter for automotive lighting: Fabrication, luminous emittance, and tunable color space," Dye. Pigment. **139**, 688–692 (2017).
15. Y. Zhou, C. Yu, E. Song, Y. Wang, H. Ming, Z. Xia, and Q. Zhang, "Three birds with one stone: K2sif6: Mn4+ single crystal phosphors for high-power and laser-driven lighting," Adv. Optical Mater. **8**, 2000976 (2020).
16. S. Arjoca, E. G. Víllora, D. Inomata, K. Aoki, Y. Sugahara, and K. Shimamura, "Ce:(ylu) alo single-crystal phosphor plates for high-brightness white leds/lds with high-color rendering (ra> 90) and temperature stability," Mater. Res. Express **1**(2), 025041 (2014).
17. T. Kang, K. Park, J. Ryu, S. Lim, Y. Yu, and J. Kim, "Strong thermal stability of lu3al5o12: Ce3+ single crystal phosphor for laser lighting," J. Luminescence **191**, 35–39 (2017).
18. M. Cantore, N. Pfaff, R. M. Farrell, J. S. Speck, S. Nakamura, and S. P. DenBaars, "High luminous flux from single crystal phosphor-converted laser-based white lighting system," Opt. Express **24**(2), A215–A221 (2016).
19. K. Park, S. Lim, G. Deressa, J. Kim, T. Kang, H. Choi, Y. Yu, Y. Kim, J. Ryu, S. Lee, and T. Kim, "High power and temperature luminescence of y3al5o12: Ce3+ bulky and pulverized single crystal phosphors by a floating-zone method," J. Luminescence **168**, 334–338 (2015).
20. T. Farooq and K. Qian, "High luminance low etendue white light source using blue laser over static phosphor," Proc. SPIE **9671**, 96710C (2015).
21. N. Abu-Ageel and D. Aslam, "Laser-driven visible solid-state light source for etendue-limited applications," J. Display Technol. **10**(8), 700–703 (2014).
22. J. Xu, A. Thorseth, C. Xu, A. Krasnoshchoka, M. Rosendal, C. Dam-Hansen, B. Du, Y. Gong, and O. B. Jensen, "Investigation of laser-induced luminescence saturation in a single-crystal yag: Ce phosphor: towards unique architecture, high saturation threshold, and high-brightness laser-driven white lighting," J. Luminescence **212**, 279–285 (2019).
23. K. Li, Y. Shi, F. Jia, C. Price, Y. Gong, J. Huang, N. Copner, H. Cao, L. Yang, S. Chen, H. Chen, and J. Li, "Low etendue yellow-green solid-state light generation by laser-pumped luag: Ce ceramic," IEEE Photonics Technol. Lett. **30**(10), 939–942 (2018).
24. X. Zhang, S. Si, J. Yu, Z. Wang, R. Zhang, B. Lei, Y. Liu, J. Zhuang, C. Hu, Y. Cho, X. Rong-Jun, Z. Hong-Wu, T. Zifeng, and W. Jing, "Improving the luminous efficacy and resistance to blue laser irradiation of phosphor-in-glass based solid state laser lighting through employing dual-functional sapphire plate," J. Mater. Chem. C **7**(2), 354–361 (2019).
25. M. H. Balci, F. Chen, A. B. Cunbul, Ø. Svensen, M. N. Akram, and X. Chen, "Comparative study of blue laser diode driven cerium-doped single crystal phosphors in application of high-power lighting and display technologies," Opt. Rev. **25**(1), 166–174 (2018).
26. Y.-P. Chang, J.-K. Chang, H.-A. Chen, S.-H. Chang, C.-N. Liu, P. Han, and W.-H. Cheng, "An advanced laser headlight module employing highly reliable glass phosphor," Opt. Express **27**(3), 1808–1815 (2019).

Optics EXPRESS

27. Y. Tang, Y. Liang, X. Ding, Q. Wu, and B. Yu, "A laser-driven phosphor converted system with enhanced optical efficiency by using light-recycling dichroic filters," J. Luminescence **223**, 117180 (2020).
28. R. Winston, J. C. Miñano, and P. Benítez, "5 - developments and modifications of the compound parabolic concentrator," in *Nonimaging Optics*, R. Winston, J. C. Miñano, and P. Benítez, eds. (Academic Press, Burlington, 2005), pp. 69–98.
29. G. Kalkowski, S. Risse, C. Rothhardt, M. Rohde, and R. Eberhardt, "Optical contacting of low-expansion materials," Proc. SPIE **8126**, 81261F (2011).
30. H. G. Stenhouse, S. J. Beecher, and J. I. Mackenzie, "Direct bonding nd: Yag to sapphire wafers," in *Laser Applications Conference*, (Optical Society of America, 2017), pp. JM5A–3.
31. C. Laboratories, "1815x refractive index liquid series m, n = 1.78," https://cargille.com/wp-content/uploads/2018/06/Refractive-Index-Liquid-Series-M-n-1.7800-at-589.3-nm-and-25%C2%B0C.pdf.
32. Synopsis, "Lighttools version 8.7.0," https://www.synopsys.com/optical-solutions/lighttools.html.
33. S. Leyre, E. Coutino-Gonzalez, J. Joos, J. Ryckaert, Y. Meuret, D. Poelman, P. Smet, G. Durinck, J. Hofkens, G. Deconinck, and P. Hanselaer, "Absolute determination of photoluminescence quantum efficiency using an integrating sphere setup," Rev. Sci. Instrum. **85**(12), 123115 (2014).
34. S. Arjoca, E. G. Víllora, D. Inomata, K. Aoki, Y. Sugahara, and K. Shimamura, "Temperature dependence of ce: Yag single-crystal phosphors for high-brightness white leds/lds," Mater. Res. Express **2**(5), 055503 (2015).
35. A. Correia, P. Hanselaer, and Y. Meuret, "Holistic opto-thermal simulation framework for high-brightness light sources based on fluorescent conversion," Opt. Express **27**(16), A1324–A1337 (2019).
36. A. Correia, P. Hanselaer, and Y. Meuret, "An efficient optothermal simulation framework for optimization of high-luminance white light sources," IEEE Photonics J. **8**(4), 1–15 (2016).
37. C. Multiphysics, "Comsol multiphysics version 5.2a," https://www.https://www.comsol.com/.
38. P. Zheng, S. Li, T. Takeda, J. Xu, K. Takahashi, R. Tian, R. Wei, L. Wang, T.-L. Zhou, N. Hirosaki, and X. Rong-Jun, "Unraveling the luminescence quenching of phosphors under high-power-density excitation," Acta Materialia **209**, 116813 (2021).
39. TheEngineeringToolbox, "Emissivity coefficient materials," https://www.engineeringtoolbox.com/emissivity-coefficients-d_447.html.
40. S. materials (FLIR), "Ce:yag material properties," http://www.scientificmaterials.com/products/ce-yag.php.
41. mt Berlin, "Sapphire (Al203)," http://www.mt-berlin.com/frames_cryst/descriptions/sapphire.htm.